PAPER

A simple collision model for small bubbles

IOP Publishing Journal of Physics: Condensed Matter
J. Phys.: Condens. Matter **29** (2017) 124005 (13pp) doi:10.1088/1361-648X/aa56fc

A simple collision model for small bubbles

Sascha Heitkam[1,3], **Anna-Elisabeth Sommer**[1], **Wiebke Drenckhan**[2] **and Jochen Fröhlich**[1]

[1] Institute of Fluid Mechanics, TU Dresden, George-Bähr-Str 3c, 01069 Dresden, Germany
[2] Laboratoire de Physique des Solides, Paris Sud XI, 91405 Orsay cedex, France

E-mail: sascha.heitkam@tu-dresden.de

Received 1 August 2016, revised 17 November 2016
Accepted for publication 5 January 2017
Published 13 February 2017

Abstract

In this work, a model for the interaction force between a small bubble and a wall or another bubble is presented. The formulation is especially designed for Lagrangian calculations of bubble or soft sphere trajectories, with or without resolution of the continuous fluid. The force only relies on position and velocity of the bubble. The model does not include any empirical parameter that would have to be calibrated. Therefore, this force model is easy to implement. The formulation of the force is explicit, which means low computational effort. The collision of a small bubble with an inclined top wall is investigated numerically and experimentally. The computational results achieved with the new collision model show good agreement with the experiment.

Keywords: bubbles, emulsions, collision, granular rheology, contact force

(Some figures may appear in colour only in the online journal)

1. Introduction

Many multiphase systems, such as fluidized sediments, emulsions, bubble columns or wet foams are dominated by the interaction of solid, liquid or gaseous particles. To simulate these systems, the forces acting between the particles or between particles and walls have to be accounted for. Interaction forces $\mathbf{F}_{\mathrm{coll}}$ result from deformation of the particles and from the pressure and velocity of the interstitial fluid. Even in phase-resolving flow simulations, the flow and pressure field are usually under-resolved in the collision zone yielding inaccurate interaction forces which are then replaced by a so-called lubrication model [13, 27]. In granular rheology simulations the interstitial fluid field is not resolved at all. Therefore, the hydrodynamic interaction forces do not result from the simulation but have to be included by additional equations.

For rigid, i.e. non-deformable, particles the deformation of the particle during collision is small and local, and is well investigated [25, 26]. Also the flow and the resulting forces can be evaluated using Stokes-flow approximations [5, 12, 19] since the particle geometry is nearly fixed. Thus, simple collision models for this class of particles exist [15]. From a numerical point of view the small contact time is critical. It should be discretized by at least 10 numerical time steps [27], in order to resolve the collision process sufficiently. Kempe *et al* [27, 29] proposed a solution to this problem by exactly conserving the kinetic energy of the particle during collision while extending the collision time.

For light, deformable particles, e.g. bubbles, these approaches are not applicable for several reasons. Due to the high deformation during collision simple deformation models lose validity. Also, the flow and pressure field in the gap between the soft bubble and the obstacle cannot be prescribed without knowing the shape of the bubble. At the same time, using a model based on the kinetic energy is not suitable, since the kinetic energy of light bubbles is small and, hence, unimportant for the collision process.

In many granular rheology simulations, the elastic collision is simplified using a spring-like collision model [17, 35, 42]

[3] This article belongs to the special issue: Emerging Leaders, which features invited work from the best early-career researchers working within the scope of *Journal of Physics: Condensed Matter*. This project is part of the *Journal of Physics* series' 50th anniversary celebrations in 2017. Sascha Heitkam was selected by the Editorial Board of *Journal of Physics: Condensed Matter* as an Emerging Leader.

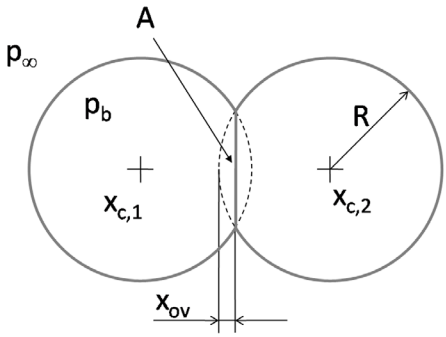

Figure 1. Sketch of the simplified collision of two bubbles, yielding a linear spring model.

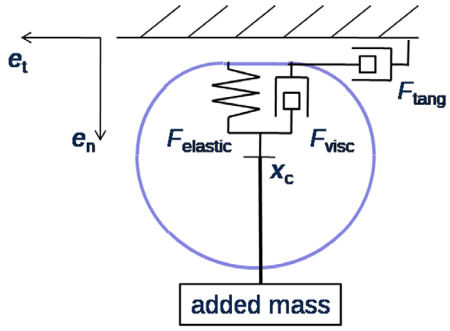

Figure 2. Equivalent network of the collision mechanics as assumed in this work. The added mass of the surrounding fluid is mounted directly to the centre position $\mathbf{x}_c$ of the bubble. Between bubble and obstacle elastic and diffusive forces appear.

$$F_{\text{coll}} = -C_s\, x_{\text{ov}}. \tag{1}$$

In this case, the collision force F_{coll} between two spheres with radius R depends linearly on the distance between the bubble centre positions $\mathbf{x}_{c,1}$ and $\mathbf{x}_{c,2}$, here used in the form of a bubble overlap $x_{\text{ov}} = 1/2|\mathbf{x}_{c,1} - \mathbf{x}_{c,2}| - R$ which would occur with spherical shapes being maintained (figure 1). The spring constant C_s is either chosen arbitrarily or, for small enough deformations, derived from surface tension σ as follows [20, 42] (figure 1). The collision force is the product of the contact area $A \approx 2\pi x_{\text{ov}} R$ and the overpressure inside a bubble $p_{\text{b}} - p_\infty = 2\sigma/R$, yielding $C_s = A(p_{\text{b}} - p_\infty) = 4\pi\sigma$. However, as shown in section 2.2 below, this collision model overestimates the stiffness of a bubble significantly. The considerable advantage of this collision model is that the force is a continuous function, easy to implement, that it requires low computational effort and that one can calculate directly the acting collision force from the bubble positions without knowing anything about the interstitial fluid, the bubble shape or the history of the collision process.

Another approach toward collision modelling of soft bubbles is the unsteady simulation of the collision zone [46]. Hendrix *et al* [21] found an elegant way to measure the lamella thickness of a bubble during the collision process using optical interference. Applying a numerical simulation of the flow field, and simultaneously of the surface shape, they found interesting numerical results on the behaviour of a lamella during collision [9, 10, 14, 33]. The essential drawback of this method is that it needs substantial computational effort to calculate a single collision. Thus, it is not suitable for simulating systems of hundreds of interacting bubbles.

In the present work, a combination of both approaches is proposed. An explicit forcing scheme, similar to equation (1) is derived, which is easy to implement, requires low computational effort and relies on well known, macroscopic parameters. The scheme is motivated by analysing the actual physics taking place in the collision zone and, hence, based on a detailed physical modelling (section 2). This model is then applied in phase-resolving simulations of small bubbles colliding with inclined walls (section 4). The same setup is investigated experimentally (section 3), providing validation with good agreement.

2. The collision model

2.1. Basic concept

We assume the interaction of the bubble with the obstacle to be purely hydrodynamic, i.e. no electrostatic forces are considered. This is justified since in the present study the lamella between bubble and obstacle remains thicker than about 10 μm (equation (14) below), which is beyond the range of electrostatic forces adressed in [30, 32] for example. During collision, the bubble remains stable, i.e. no coalescence or rupture takes place. The obstacle can be a flat plate or another bubble of comparable size. In this work, the analytic estimations, experiments and simulations are carried out for the interaction of a bubble with a flat plate. At the same time a variant for bubble–bubble collision is obtained by with slight changes in some constants. This is expressed in the corresponding sections below. The hydrodynamic collision force is assumed to consist of three contributions: a normal elastic force F_{elastic}, a normal viscous force F_{visc} and a tangential viscous force F_{tang}, depicted in figure 2. The concept of a spring-dashpot model for the modeling of collision forces is well known in molecular dynamics and dissipative particle dynamics. However, usually a linear spring and a linear dashpot is applied [7, 8, 22, 45]. In the present work we want to provide a nonlinear, physically motivated behaviour of spring and dashpot. For each element in figure 2 models are derived below. To do so, an axisymmetric deformation of the bubble is assumed. The normal viscous and the tangential viscous forces both result from the dissipative flow of the liquid. Due to the low Reynolds number in the collision zone, nonlinear inertia effects are neglected and an undisturbed superposition of both velocity fields is assumed. In other words, the normal and the tangential collision process are considered to be independent from each other. Also, interaction of several collisions that may occur at the same time is neglected.

From a conceptual point of view it is important to stress the following. The simulations using the proposed model are

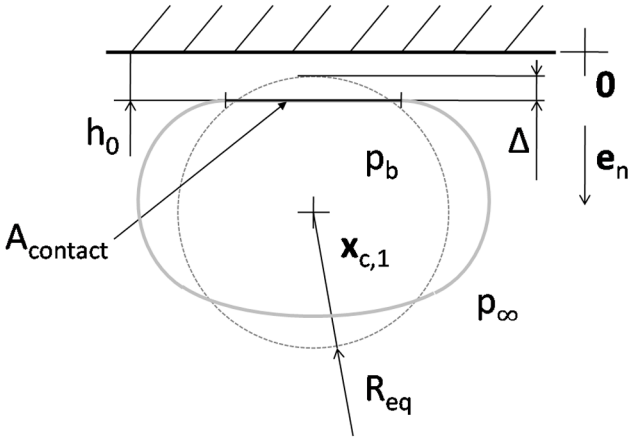

Figure 3. Relation between undeformed spherical bubble, as it is assumed by the numerical simulation, and deformed bubble in the collision model. The centre of mass $\mathbf{x}_c$ and the bubble volume are considered to be the same. The distance deficit Δ is the amount of deformation at the side of the obstacle.

conducted assuming constant spherical shape of the bubbles which move according to the various forces exerted on them. To derive these forces specific deformations are assumed and analysed, as in figures 3 and 4, etc. But these deformations are only employed to derive realistic interaction forces, and this is the way they are accounted for. They are not reflected by the shape of the numerical objects in the simulation which remain spherical. It is this duality which makes the resulting simulation highly efficient while physically realistic on the other hand.

2.2. Elastic normal force

Similar to the overlap in the spring model, a distance deficit Δ is defined as shown in figure 3. It results from comparing the deformed bubble with a sphere of the same volume, that is the same equivalent radius $R_{\mathrm{eq}}^3 = 3V_{\mathrm{b}}/4\pi$, and the same centre of mass. The amount the sphere is deformed by the obstacle is represented by Δ, the deficit in distance to the obstacle. It can be related to the position of the bubble by

$$\text{Particle}: \ \Delta = R_{\mathrm{eq}} - 1/2|\mathbf{x}_{c,1} - \mathbf{x}_{c,2}| + h_0/2 \tag{2}$$

$$\text{Wall}: \ \Delta = R_{\mathrm{eq}} - \mathbf{x}_{\mathrm{c},1} \cdot \mathbf{e}_{\mathrm{n}} + h_0, \tag{3}$$

involving also the thickness h_0 of the fluid film between the bubble and the obstacle. For the elastic force, this film thickness can either be neglected or approximated with equation (14) below.

Elastic normal forces F_{elastic} result from variation of the surface energy E_{s} of the bubble due to deformation of the bubble when colliding with an obstacle. Thus, it can be derived by calculating the shape of a bubble during a collision process. The force then results from the total surface area A_{b}, the surface tension σ and the distance deficit Δ of the bubble according to

$$F_{\mathrm{elastic}} = \frac{\mathrm{d}E_{\mathrm{s}}}{\mathrm{d}\Delta} = \sigma\frac{\mathrm{d}A_{\mathrm{b}}}{\mathrm{d}\Delta}. \tag{4}$$

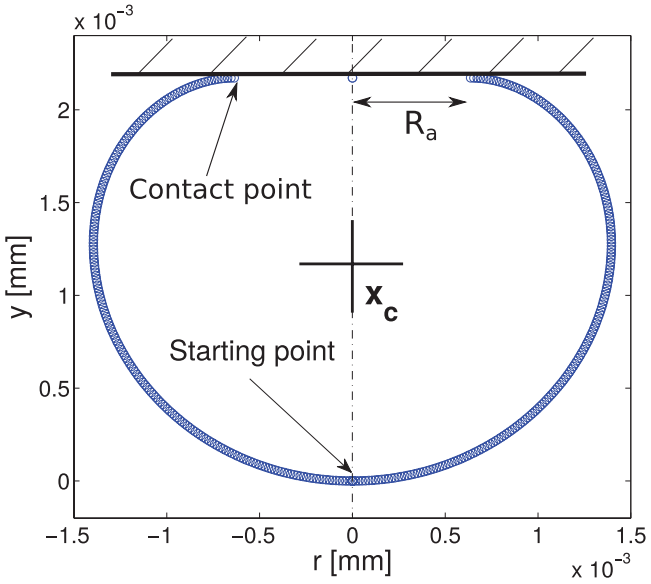

Figure 4. Numerical result of the shape of a bubble colliding with a horizontal wall.

The shape of the bubble is computed point-wise in an iterative procedure to fulfil the Young–Laplace law [6] comparing the mean curvature H_{m}, the external fluid pressure distribution p_{out} and the internal bubble pressure p_{b}, which is assumed constant all over the bubble volume

$$p_{\mathrm{b}} - p_{\mathrm{out}} = \sigma\left(\frac{1}{R_\alpha} + \frac{1}{R_\beta}\right) = \sigma H_{\mathrm{m}}. \tag{5}$$

A typical result for a computed shape is shown in figure 4. Technical details on the shape calculation can be found in appendix A.

The fluid force distribution p_{out}, acting on the bubble depends on the dynamic collision process, and the instantaneous flow and pressure field around the bubble. With the above algorithm, however, an equilibrium state is assumed. It is now investigated to which extend unknown fluctuations of p_{out} might influence the result. This is done by considering different functions $p_{\mathrm{out}}(y, r)$

$$p_{\mathrm{out}} = p_s - \rho_f g y \tag{6}$$

$$p_{\mathrm{out}} = p_s + \begin{cases} 0.5\rho_{\mathrm{f}} q_{\mathrm{ref}}^2, & \text{lower hemisphere} \\ 0, & \text{upper hemisphere} \end{cases} \tag{7}$$

$$p_{\mathrm{out}} = p_s + \begin{cases} \dfrac{3\mu_{\mathrm{f}} q_{\mathrm{ref}}}{2R_{\mathrm{eq}}}\cos\theta, & \text{lower hemisphere} \\ 0, & \text{upper hemisphere} \end{cases}. \tag{8}$$

Equation (6) corresponds to a hydrostatic situation, equation (7) to a constant dynamic pressure on the lower hemisphere of the bubble, and equation (8) to the solution of an upward potential flow with q_{ref} around the lower hemisphere, where $\theta = 2\arctan(y/r)$. In case of equations (7) and (8) on the upper hemisphere, p_{out} equals p_s.

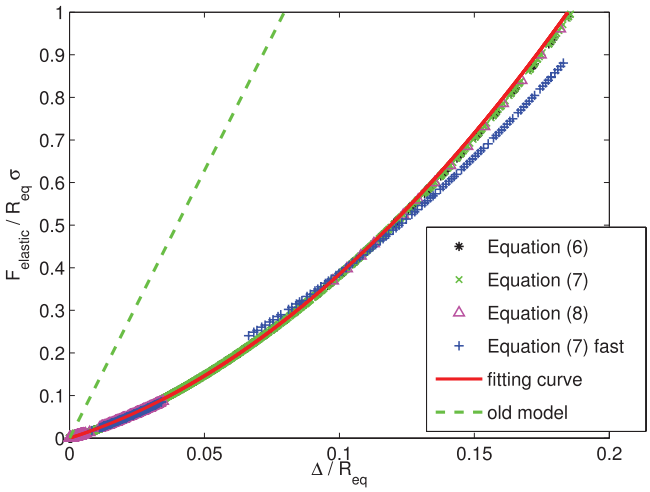

Figure 5. Relation between elastic collision force F_{elastic} and the distance deficit Δ between the centre of mass of a bubble and the obstacle for different force distributions (symbols). The solid line is the fitting curve according to equation (9). The dashed line shows the basic collision model from equation (1).

In these different distributions of p_{out} physically reasonable parameters are employed. The velocity q_{ref} is set to the undisturbed rising velocity of bubbles with equivalent radius $R_{\text{eq}} = 0.5 \ldots 3$ mm in water with viscosity μ_{f}.

From the variation of p_{out} it is found, that the deformation of the bubble is, for physically reasonable distributions of p_{out}, only weakly dependant on the distribution but essentially only on the integral value F_{out}. Figure 5 shows the total fluid force F_{out} against the relative deficit of distance to the wall $\Delta/R_{\text{eq}} = (R_{\text{eq}} - \mathbf{x}_{\text{c}} \cdot \mathbf{e}_{\text{n}})/R_{\text{eq}}$ for a deformed bubble, combined from several computations with different bubble parameters and force distributions $p_{\text{out}}(y, r)$. Obviously, different distributions of p_{out} collapse on the same graph. The blue + symbols that do not fit in so well correspond to equation (7) with an artificially high velocity of $10 \times q_{\text{ref}}$. The other results are well represented by the fitting curve

$$\frac{F_{\text{elastic}}}{R_{\text{eq}}\sigma} = 18.5\left(\frac{\Delta}{R_{\text{eq}}}\right)^2 + 2.0\frac{\Delta}{R_{\text{eq}}}. \tag{9}$$

This expression for the elastic force only involves the bubble position, its radius and the surface tension. It can be computed explicitly and is thus easy to implement and, most of all, requires low computational effort. The spring-like collision model described in the introduction is also shown in figure 5(broken line). It overestimates the stiffness of a bubble because it does not allow for relaxation from the prescribed collision shape in figure 1

These elastic simulations also yield the relation between Δ and R_a, which are also nearly independent of the character of p_{out}. The relation can be fitted by

$$\frac{\Delta}{R_{\text{eq}}} = 2.36\left(\frac{R_a}{R_{\text{eq}}}\right)^2 + 0.04\frac{R_a}{R_{\text{eq}}}. \tag{10}$$

This result will be used in the next part.

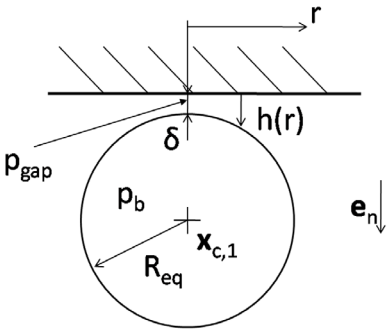

Figure 6. Sketch of the geometry of the gap when a spherical particle approaches a wall.

2.3. Thickness of fluid lamella

If a spherical particle moves normal to an obstacle with the relative velocity $u_{\text{c}} = -\dot{\mathbf{x}}_{\text{c}} \cdot \mathbf{e}_{\text{n}}$, additional forces occur due to fluid interaction between particle and obstacle. Cox and Brenner [12] derived an expression for this lubrication force, solving the equations for Stokes flow between a plane wall and a spherical particle with distance δ between its surface and the wall

$$F_{\text{viscous}} = -6\pi\mu_{\text{f}}\dot{\mathbf{x}}_{\text{c}} \cdot \mathbf{e}_{\text{n}} R_{\text{eq}} \frac{R_{\text{eq}}}{\delta}. \tag{11}$$

However, this expression loses validity if the particle is deformable, e.g. a bubble, and the lubrication force becomes very high. To estimate the limit of its validity, the pressure in the gap between sphere and wall can be used. Figure 6 sketches the geometry of the problem. The width of the gap is

$$h(r) = \delta + R_{\text{eq}} - \sqrt{R_{\text{eq}}^2 - r^2}. \tag{12}$$

The overpressure $p_{\text{gap}} - p_\infty$ in the centre of the gap between particle and wall can be calculated by integrating the pressure gradient from outside to the centre [12] yielding

$$p_{\text{gap}} - p_\infty = \frac{3}{2}\mu_{\text{f}}u_{\text{c}}\int_{R_{\text{eq}}}^{0}\frac{-r}{h^3(r)}\,\mathrm{d}r \approx \frac{3}{2}\mu_{\text{f}}u_{\text{c}}\frac{R_{\text{eq}}}{2\delta^2}. \tag{13}$$

When a deformable bubble approaches a wall and when the pressure in the gap reaches the pressure inside the bubble, the surface between them decelerates. Consequently, the viscous force then becomes much smaller than equation (11) suggests. The gap width h_0 at which gap pressure and pressure inside the bubble are equal, can be derived from equation (13)

$$p_{\text{gap}} - p_\infty \approx \frac{3}{2}\mu_{\text{f}}u_{\text{c}}\frac{R_{\text{eq}}}{2h_0^2} = \frac{2\sigma}{R_{\text{eq}}}$$

$$h_0 = \begin{cases} \sqrt{\frac{3}{8}}\sqrt{\mu_{\text{f}}u_{\text{c}}\frac{R_{\text{eq}}^2}{\sigma}}, & \text{bubble–wall} \\ \sqrt{\frac{3}{16}}\sqrt{\mu_{\text{f}}u_{\text{c}}\frac{R_{\text{eq}}^2}{\sigma}}, & \text{bubble–bubble.} \end{cases} \tag{14}$$

For bubble–bubble collisions a different pre-factor results due to the different shape of $h(r)$. The gap width h_0 has to be used in equation (3) when computing the distance deficit. But it is even more important when estimating the viscous force

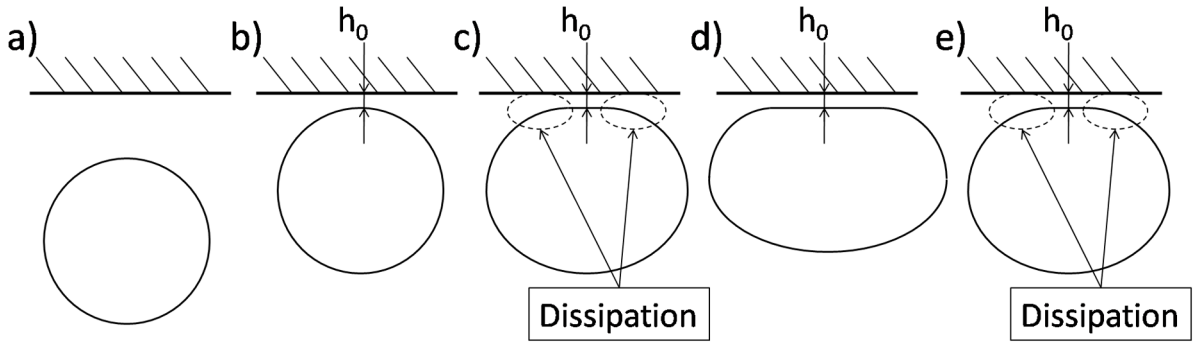

Figure 7. Proposed simplification of the collision process. (a) The bubble remains spherical while approaching an obstacle. (b) When the pressure in the gap equals the inner pressure of the bubble, the corresponding gap width h_0 is frozen. (c) Further approach of the bubble corresponds to deformation of the bubble, where the gap width remains constant while the gap area increases and liquid is displaced in the dissipation zone. (d) After reaching its minimum distance the process is reversed (e).

below, because for zero gap width an infinite viscous force would result. For better numerical stability it might be practical to set a lower bound for the gap width, motivated by the disjoining pressure between obstacle and particle [6].

2.4. Viscous normal force

To derive the viscous force, one needs to calculate the flow inside the gap. To do so, one also needs to calculate the shape of the lamella [33], which, again, results from the flow inside and outside the lamella. This ends up in a very complex problem. Here, instead, a simplification of this problem is proposed, sketched in figure 7, which allows an analytic solution of the energy dissipation inside the dissipation zone. The analytic solution bases on three assumptions: (i) A no-slip condition is valid on the bubble surface (contaminated fluid) and on the obstacle surface. (ii) Tangential movement does in average not influence the dissipation caused by the normal movement. (iii) The obstacle is either a plane wall or another bubble of similar radius.

The collision process looks as follows. A spherical bubble approaches a wall and maintains its spherical shape until the pressure in the gap equals the inner pressure of the bubble. Now, the gap width $\delta = h_0$ is frozen and deformation takes place, according to figure 4. After reaching stagnation, the bubble movement is reversed. The deformation of the bubble causes energy dissipation due to the viscous flow of the displaced liquid in the collision zone. However, since the gap width h_0 is constant in time, there is no dissipation in the lamella itself but only near its rim, as indicated in figure 4. To support this idea an upper bound for the energy dissipation $\Delta E_{\max}$ is estimated, that could take place inside the lamella if the whole lamella volume $V_{\max}$ is displaced with the maximum over-pressure $\Delta p_{\max}$, yielding

$$\Delta E_{\max} = \Delta p_{\max} V_{\max} = \frac{2\sigma}{R_{\mathrm{eq}}} \pi R_a^2 h_0. \tag{15}$$

For a gas bubble with $R_{\mathrm{eq}} = 1$ mm rising in water and colliding with a horizontal wall, yielding an assumed contact area radius R_a of $R_a \approx R_{\mathrm{eq}}/2 = 0.5$ mm, $\Delta E_{\max}$ would equal about 2×10^{-9} J. However, the typical kinetic energy $E_{\mathrm{kin,b}}$ of such a bubble and the surrounding fluid is

$$E_{\mathrm{kin}} = \frac{4}{3} \pi R_{\mathrm{eq}}^3 \rho_{\mathrm{f}} C_{\mathrm{am}} \frac{q_{\mathrm{ref}}^2}{2}. \tag{16}$$

With an added-mass coefficient C_{am} of 1/2 and a rise velocity q_{ref} of 0.24 m s^{-1} this would equal about 4×10^{-8} J, which is 20 times bigger than the maximum dissipation in (15). Thus, thinning of the lamella seems to be negligible when estimating the dissipative collision force. Combining equation (B.5) and the equations (B.12), (B.13), (B.3) and (B.4), one ends up with an expression for the viscous force, acting on a bubble in the collision process

$$F_{\mathrm{viscous}} = u_{\mathrm{c}} C_{\mathrm{bc}} \frac{12\mu_{\mathrm{f}}}{2\pi} 0.34 \left(\frac{\Delta}{R_{\mathrm{eq}}} + 0.0002 \right)^{-0.5} \times \left(4.0 \sqrt{\frac{R_{\mathrm{eq}}^3}{h_0}} + 3.0 R_a \frac{R_{\mathrm{eq}}}{h_0} \right). \tag{17}$$

The parameter C_{bc} represents the collision partner. For a bubble–wall collision holds $C_{\mathrm{bc}} = 1$, for for a bubble–bubble collision $C_{\mathrm{bc}} = 1/4$. This expression only involves the deformation Δ of the bubble, bubble velocity u_{c}, bubble radius R_{eq} and fluid viscosity μ_{f}. The thickness of the lamella, h_0, can be estimated with equation (14). The contact radius R_a is given by equation (B.4) and only depends on R_{eq} and Δ, as well. The force is a linear function of the bubble velocity, which is typical for viscous dissipation mechanisms. If the distance between bubble and wall is larger than h_0, equation (17) does not yield plausible results, so that the following scheme of (table 1) is applied.

Table 1. Scheme for switching between stokes flow dissipation and the present method.

Distance	Method
$\mathbf{x}_{\mathrm{c}} \cdot \mathbf{e}_{\mathrm{n}} - R_{\mathrm{eq}} > h_0$	Equation (11)
$\mathbf{x}_{\mathrm{c}} \cdot \mathbf{e}_{\mathrm{n}} - R_{\mathrm{eq}} < h_0$	Equation (17)

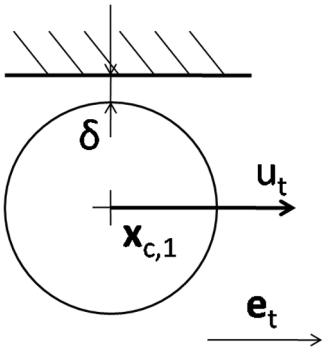

Figure 8. Geometry of a spherical bubble moving tangential to a wall or obstacle.

After the bubble centre reaches its closest position to the wall, its movement is reversed. The dissipation process described above can be assumed to take place in reverse order. While the bubble withdraws from the obstacle, liquid is sucked into the lamella, an under-pressure is generated in the dissipation zone. Due to this under-pressure, the surface shape supposedly looks different than during the approach of the bubble, but this is not taken into account here. Instead, the geometry is assumed to be described by figure B1 as well. The reversed Poiseuille flow then dissipates energy according to the same mechanism, leading to exactly the same equation (17) for the dissipative force F_{visc} as in the approaching process. The negative sign is provided now by the negative normal velocity u_{c} in the equation. Also, the process of detachment between bubble and obstacle is presumably different during the withdrawal of the bubble. But again, this is not taken into account here. When approaching, the bubble has a much larger normal velocity, resulting in higher energy dissipation than during withdrawal of the bubble. Therefore, lower accuracy in modelling the withdrawal process should not influence the overall process too much. Finally, it was checked, that the dissipation modelled by (17) is of the order of E_{kin} in (16) and hence, much larger than the dissipation in the lamella (15), so that replacing the latter is justified indeed.

2.5. Tangential force

When a bubble moves parallel to a wall with the velocity $u_{\mathrm{t}} = \dot{\mathbf{x}}_{\mathrm{c}} \cdot \mathbf{e}_{\mathrm{t}}$, there is an additional friction force, acting on the bubble. This situation is sketched in figure 8. Goldman *et al* [19] developed an equation for this force, assuming Stokes flow

$$F_{\mathrm{tang}} = \frac{16}{5}\pi\mu_{\mathrm{f}}u_{\mathrm{t}}R_{\mathrm{eq}}\ln\left(\frac{\delta}{R_{\mathrm{eq}}}\right). \tag{18}$$

In the present collision model, the distance δ between the undeformed bubble and the wall is somewhat problematic, because the modelling of the normal collision force does not exclude a negative value of δ (see discussion in section 2.1 above). Thus, using directly the distance δ can result in undefined values for the logarithm in equation (18). To estimate a value for δ, equation (14) could be used. However, if the bubble does not impact but slides along the wall, the velocity

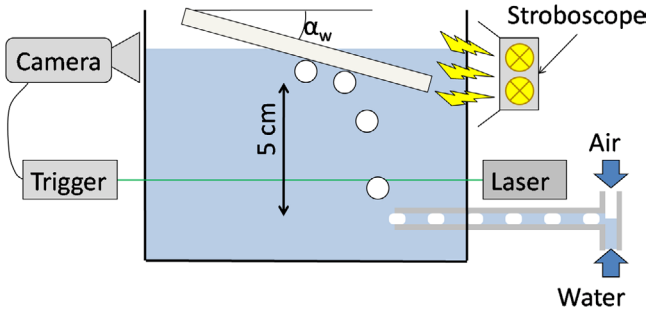

Figure 9. Experimental setup for measuring the trajectory of a bubble colliding with an inclined plane.

of the bubble normal to the wall, which is required in equation (14), is not well defined. For this reason, a lower limit for δ is used here,

$$\delta = \max(\mathbf{x}_{\mathrm{c}} \cdot \mathbf{e}_{\mathrm{n}} - R_{\mathrm{eq}}, 10\ \mu\mathrm{m}). \tag{19}$$

The value of 10 μm is chosen as a typical minimum lamella thickness, taken from [21]. If the bubble is far away from the wall, δ becomes larger than R_{eq} and equation (18) yields positive values. This is physically incorrect and equation (18) has to be switched off.

3. Experiment for inclined bubble collision

3.1. Motivation

For validation, experiments with a bouncing bubble were carried out. In the literature one can find data for the trajectory of a bubble colliding with a wall [36–38, 41, 43, 47, 48]. However, these experiments usually investigate large bubbles undergoing strong deformations during the collision. Also, clean water is used most often, leading to a free-slip condition at the bubble surface. Thus, no literature data was found that could be used to validate the collision model derived above. Therefore, it was decided to design an experiment in order to have complete control of all parameters and to investigate configurations that correspond to the assumptions made above.

3.2. Experimental setup

Figure 9 shows the experimental setup. Single bubbles are introduced into soapwater at the bottom of a container. As a surfactant, 25 cm^3 soap (german dish washing soap 'FIT') were added to 5000 cm^3 water, leading to a highly contaminated bubble surface. Thus, the no-slip condition at its surface is valid [11]. The experimental parameters are given in table 2.

Small, monodisperse bubbles are created and transported into the fluid with a special microfluidic device [18]. They rise, reach terminal velocity and collide with the inclined plane. Before doing so they pass a light barrier which triggers the photo camera. Instead of taking a sequence of images, a stroboscope was employed. It emits several flashes within one camera exposure time. Consequently, the same bubble appears four times on one picture. A sample picture is shown in figure 10. For each setup, approximately 5000 pictures

Table 2. Geometry, material and optical parameters for the measurements of the collision process of a small bubble with an inclined plane.

Parameter	Value
Boxsize	$20 \times 20 \times 20$ cm^3
Bubble radius	0.6 … 0.8 mm
Collision angle	20 … 45°
Material	Highly contaminated water
Fluid viscosity	10^{-3} Pa s
Fluid density	10^3 kg m^{-3}
Surface tension	0.030 ± 0.005 N m^{-1}
Optical resolution	20 μm
Flash rate	250 s^{-1}
Flash length	100 μs
Exposure time	1/60 s
Bubble rate	1 s^{-1}

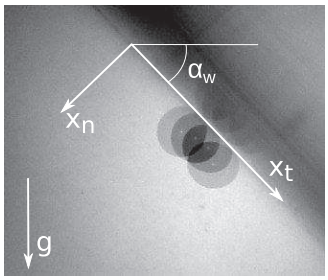

Figure 10. Sample image of a bubble ($R_{eq} = 0.6$ mm) colliding with an inclined plane ($\alpha_w = 45°$).

were taken. These images were processed by applying edge filtering and a correlation-based detector for round objects, yielding the centre of mass x_i and an intensity I_i for each bubble image i within one picture. The velocity was extracted using a central difference approach

$$u_i = \frac{x_{i+1} - x_{i-1}}{2\, t_{\text{flash}}}. \tag{20}$$

The mean intensity $\bar{I} = (I_{i-1} + I_i + I_{i+1})/3$ is a measure for the image quality of the bubble sequence. Events with a mean intensity lower than the average value of $\bar{I}$, taken from all pictures, are discarded.

3.3. Experimental results

The inclination angle α_w of the plane wall and the bubble radius R_{eq} of the bubble were varied as indicated in table 2. For a tilt α_w above $\approx 60°$ as well as for a bubble radius below $R_{eq} \approx 0.4$ mm the bubble smoothly propagates towards and along the wall without showing characteristic features in the trajectories, e.g. rebound. With increasing values of α_w or R_{eq}, a rebound after collision and a re-acceleration become more prominent in experiment and simulation, making the comparison more meaningful. However, for α_w above 45°, the collision point varies from bubble to bubble, resulting in a blurred measurement of the trajectory. At the same time, the ascension path of larger bubbles fluctuates, again resulting in an unsharp trajectory. Therefore, even though a large

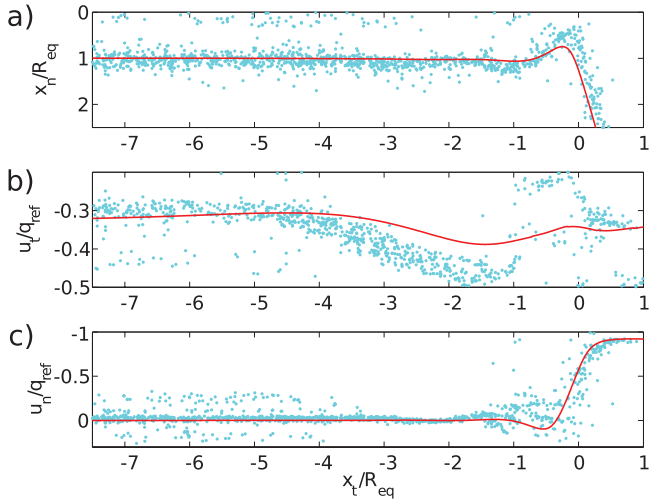

Figure 11. Experimental (points) and numerical (line) results of normal position (a), tangential velocity (b) and normal velocity (c) of a bubble with $R_{eq} = 0.6$ mm, colliding with a plane, inclined by $\alpha_w = 20°$, as a function of the tangential position.

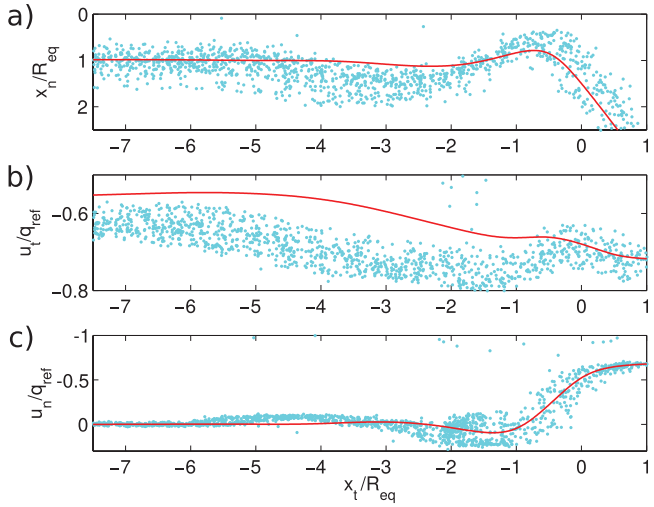

Figure 12. Experimental (points) and numerical (line) results of normal position (a), tangential velocity (b) and normal velocity (c) of a bubble with $R_{eq} = 0.8$ mm, colliding with a plane, inclined by $\alpha_w = 45°$, as a function of the tangential position.

variety of parameters was investigated, only a bubble radius $0.6\text{ mm} \leqslant R_{eq} \leqslant 0.8$ mm is considered here and the inclination angle is limited to the interval $20° \leqslant \alpha_w \leqslant 45°$.

Figures 11 and 12 show experimental results: the wall distance, the normal velocity and the tangential velocity of the bubbles centre of mass. The data show a significant scatter. Each point corresponds to a different bubble and the scatter is caused by small variations in the trajectory and the radius of consecutive bubbles.

4. Validation of the collision model

4.1. Numerical method

The experimental situation investigated in section 3 is now simulated by a particle-resolving method employing the new collision model proposed in section 2. This is done with the

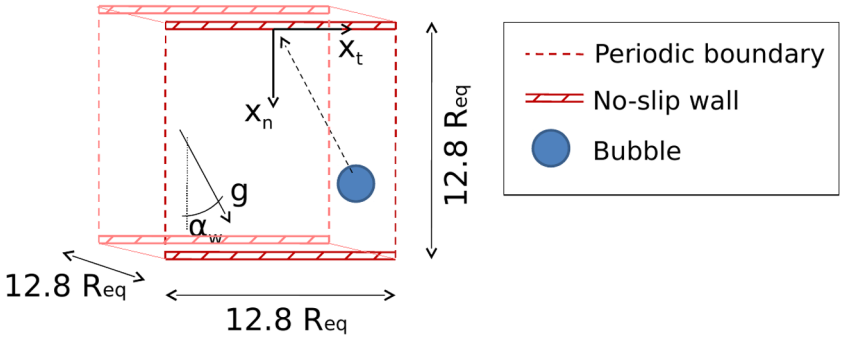

Figure 13. Numerical setup for the investigation of the collision of a bubble with a wall, tilted by the angle α_w with respect to the gravitational acceleration.

immersed-boundary method (IBM) developed by Kempe and Fröhlich [28]. It features a Navier–Stokes solver for incompressible flow on a staggered Finite-volume grid with a Runge–Kutta scheme containing a pressure correction equation. The method is of second order accuracy in both space and time. Spherical particles of diameter larger than the step size Δs of the background grid are propagated by solving an ordinary differential equation in time for each particle. As the bubbles considered here have close to vanishing mass the stabilized time scheme of Schwarz *et al* [39] is used.

The forces generating the bubble motion are of two kinds. Fluid dynamic forces on length scales larger than Δs are resolved. The two-way interaction between fluid and bubble is numerically realized with the IBM [28] employing regularized delta functions for interpolation and spreading of information from the particle boundary to the background grid. This information is generated at n_L so-called Lagrangian marker points regularly distributed over the bubble surface. The collision forces of section 2 represent effects not resolved by the spatial discretization and the conserved spherical bubble shape. The lubrication model employed in other studies with solid particles [27] is not used here.

4.2. Simulated configuration

The collision of a small bubble ($R_\mathrm{eq} = 0.6$ mm) with an inclined plate ($\alpha_w = 20° \ldots 45°$) was simulated with three different collision models. The setup is shown in figure 13. The initial condition is quiescent fluid and the bubble is unleashed at a distance of $11.3R_\mathrm{eq}$ from the wall. The applied collision models are given in table 3 and the numerical parameters in table 4.

4.3. Simulation results and comparison

In a first step the new collision model is investigated on its own assessing the importance of the different contributions. To this end, the collision is simulated with different terms of the collision model switched on and off, as indicated in table 3. The wall distance, the normal velocity and the tangential velocity of the bubble obtained from the three variants are plotted over the wall-parallel coordinate x_t of the bubble center in figure 14.

Table 3. Applied terms of the collision force for the comparison of three different collision models.

Case	F_elastic	F_visc	F_tang
Elastic spring model	$4\pi\sigma\Delta$	—	—
Visco-elastic normal forces	Equation (9)	Equation (17)	—
Full new model	Equation (9)	Equation (17)	Equation (18)

Table 4. Parameters for the simulation of a bubble colliding with a tilted wall.

Quantity	Symbol	Value
Domain size	$L_x \times L_y \times L_z$	$12.8R_\mathrm{eq} \times 12.8R_\mathrm{eq} \times 12.8R_\mathrm{eq}$
Bubble radius	R_eq	0.0006 m
Fluid viscosity	μ_f	10^{-3} Pa ∗ s
Fluid density	ρ_f	10^3 kg m^{-3}
Surface tension	σ	0.03 N m^{-1}
Reynolds number	Re	280
Eötvös number	Eo	0.48
Spatial resolution	Δs	6×10^{-5} m
Time step	Δt	10^{-4} s
Lagrange points	n_L	1258
Tilt angle	α_w	$20° \ldots 45°$

Obviously, the classic elastic spring model (dash-dotted red line) leads to oscillating movement in the normal position. Using the elastic model (9) and the viscous dissipation term (17) results in a smoother path. Only one small rebound occurs. Including the tangential force term (18) barely affects the normal position and velocity but leads to a different tangential velocity after collision.

The essential issue now is to carry out simulations with the full new collision model and to compare the simulation results with the experimental data. This is done in figures 11 and 12. In the experimental data of the velocities, equation (20) causes a low-pass-filtering of the velocities. In order to ensure better comparability, the numerical data was treated equally.

Experiment and simulations show fairly good agreement. The penetration depth, the rebound height and the corresponding time scales agree to a very reasonable amount. The simulation reproduces the fact that there is only a short contact

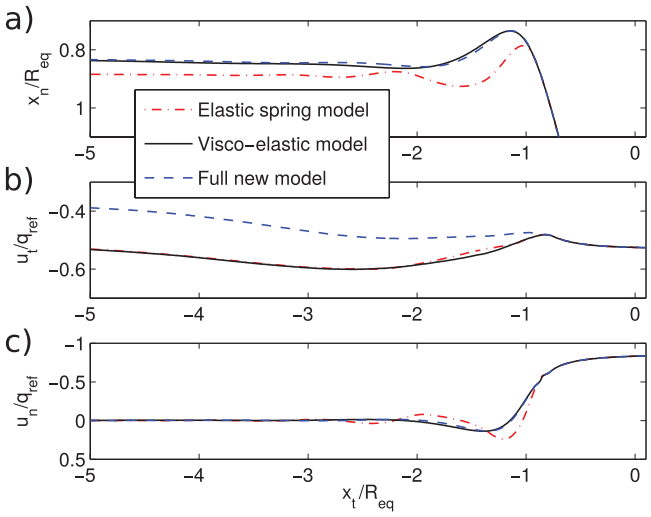

Figure 14. Comparison of different collision models. Normal centre position (a), tangential (b) and normal (c) velocity of a bubble ($D = 1.2$ mm), colliding with an inclined plane ($\alpha_w = 30°$) as a function of the tangential position. In time, the bubble follows the curves from right to left. Different variants of the model with certain parts of the model switched on and off according to table 3 are compared.

time and nearly no rebound at low angle, while at higher angle longer contact times and a rebound take place.

The tangential velocity shows agreement in the general trends. In simulation as well as in experiment, one can see the deceleration in the moment of impact, the partial acceleration during the rebound and then a slow declaration towards the terminal tangential velocity. Oscillations, as predicted by the spring model in figure 14 do not take place.

Of course, the agreement between experiment and simulation is not perfect, but one has to keep in mind that the advanced collision model does not include any empirical parameter that potentially could be used to calibrate the collision model for better agreement with the experiment. Furthermore, the new model provides a substantial improvement of the result compared to the spring model widely used.

5. Conclusions

In this work, a model for the collision force, acting between a bubble and a wall or another bubble was derived. To apply this model, one does not need to know anything about pressure or velocity of the fluid in the gap between bubble and obstacle. The model only requires position and velocity of the bubble. It is also free of empirical parameters that would have to be calibrated in order to represent reality. Instead, parameters are derived from material properties and physical approximations.

Of course, this simple model does not reproduce the interaction of densely packed bubbles and droplets perfectly. The comparison with the experiment has revealed deviations in the tangential velocity. Other, more complex models for the tangential viscous force [3, 31] might be more realistic. Also, it is known that multiple contacts of a single bubble interact with each other in a nonlinear way [34]. One can find surface evolver simulations [4] that compute and model the nonlinear interaction potential of densely packed bubbles with a very high accuracy [23]. Also for the dissipative forces more detailed and complex investigations are available [16, 40]. But despite these highly sophisticated models, many researchers [2, 24, 44] use the elastic spring model proposed by Durian [17] because it requires low computational effort, is easy to implement, and performs robust.

Comparing our new model with the classical spring-like collision model reveals a significant difference in our scenario, due to the higher stiffness and the absence of dissipation in classical model. The spring-like model results in stronger oscillations after the bubble impact which have not been reproduced by the validation experiment. These oscillations might lead to arbitrary movements within a cluster of bubbles. Therefore, it is questionable to use the spring model for small, soft particles or bubbles.

Instead we suggest to use the present model, since it requires only slightly more computation power (approx. 15 % in our case), is very easy to implement in any discrete element code or Euler-Lagrange method, and yields higher physical realism. For simulations of interacting soft particles without interstitial liquid we suggest to use at least the new approximation of the elastic normal force (equation (9)) instead of a spring-like collision model since the latter highly overestimates the stiffness of bubbles or droplets.

Acknowledgment

We gratefully acknowledge fruitful discussions with Nikolai Denkov. Computation time was provided by the ZIH Dresden. This work was partially funded by the German Research Foundation (HE 7529/1-1), by the European Research Council (ERC, FP7/2007-2013, 307280-POMCAPS) and by the Helmholtz Society via the LIMTECH Alliance, project A5.

Appendix A. Shape computation

The shape of the bubble is computed point-wise in an iterative procedure of letting the principal curvatures R_α and R_β converge to a predescribed target. The target results from the Young–Laplace law [6] comparing the external fluid pressure distribution p_{out} and the internal bubble pressure p_{b}, which is assumed constant all over the bubble volume, and relating the difference to the mean curvature H_{m}

$$p_{\text{b}} - p_{\text{out}} = \sigma\left(\frac{1}{R_\alpha} + \frac{1}{R_\beta}\right) = \sigma H_{\text{m}}. \qquad \text{(A.1)}$$

The pressure distribution p_{out} depends on the position along the bubble surface and is not known, but assumed according to basic fluid mechanics. It will be demonstrated below, that the actual distribution of p_{out} does not have a large influence. For a starting point one may assume a purely gravitational outer pressure field $p_{\text{out}}(y) = p_s - \rho_{\text{f}} g y$, with g the gravity, p_s the pressure at the lowest point of the bubble and y the coordinate pointing upward from this lowest point. The shape of a bubble

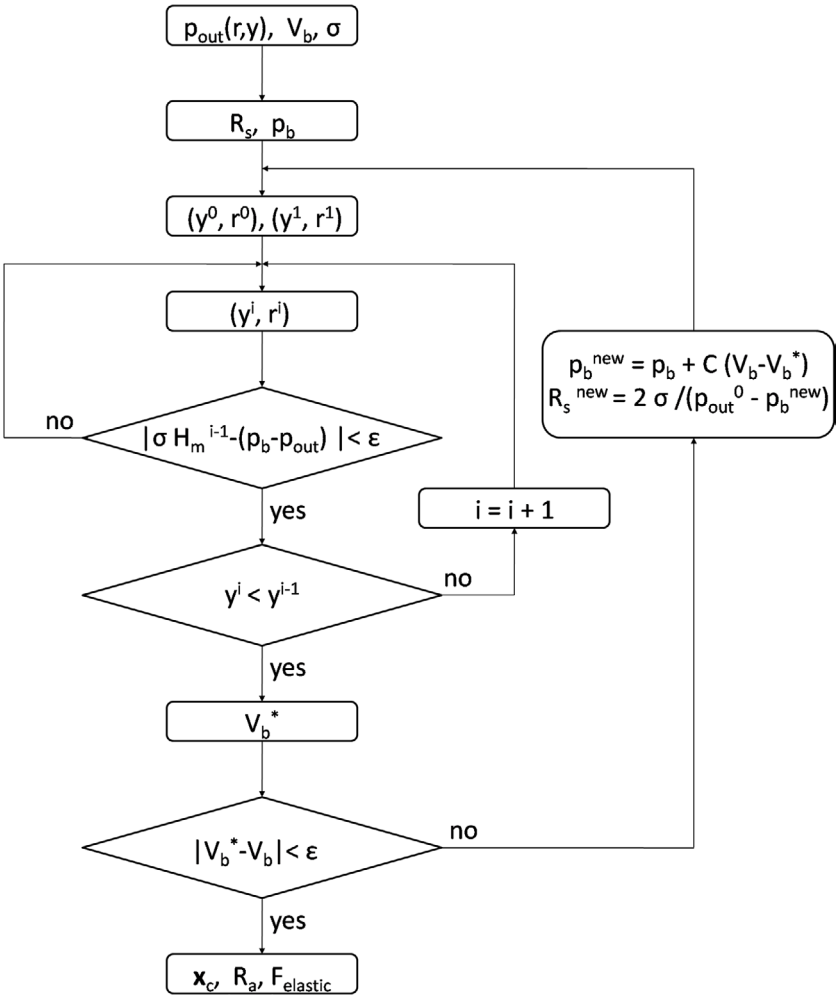

Figure A1. Flow chart of the procedure for determination of the shape of a bubble in contact to a horizontal wall. An inner iteration ensures that each surface point i fulfills equation (A.1) to a small residuum e. An outer iteration controls the bubble volume V_b.

with a certain volume V_b is to be computed. Figure A1 gives the flow chart for the iteration. From

$$R_s = (3V_\mathrm{b}/4\pi)^{1/3}, \tag{A.2}$$

a starting guess R_s for the curvature radius at the apex is derived. From R_s a starting value for the bubble pressure $p_\mathrm{b} = 2\sigma/R_s$ is derived. Also the step width for the point-wise computation $s_s = R_s/1000$ is chosen based on R_s (figure A2).

Now, the computation starts at the lowest point of the bubble, marked in figure 4. The coordinates of this point are assigned to be $(y^0, r^0) = (0, 0)$. The second point (y^1, r^1) results from the imposed curvature at the first point, R_s, the distance, s_s, and symmetry, as sketched in figure A2, giving

$$y^1 = s_s^2/(2R_s) \tag{A.3}$$

$$r^1 = s_s\sqrt{1 - y^1/(2R_s)}\,. \tag{A.4}$$

After knowing the first two points, each of the subsequent points (y^i, r^i) can be calculated by a central difference approach with the help of the last two points (y^{i-1}, r^{i-1}) and (y^{i-2}, r^{i-2}). The mean curvature H_m^{i-1} can be derived from the three points (i),$(i-1)$, and $(i-2)$ assuming the surface to be a regular patch $\mathbf{x} : (r, y) \rightarrow \mathfrak{R}^3$ parametrisised by r and y

$$H_\mathrm{m} = \frac{eG - 2fF + gE}{2(EG - F^2)}, \tag{A.5}$$

where E, F and G are the coefficients of the first fundamental form and e, f and g the coefficients of the second fundamental form of the parametrisation. Derivatives of the parameterization are approximated, using a central difference approach in the point (y^{i-1}, r^{i-1}). More information on the calculation of the curvature and the detailed equations are given in [1]. The mean curvature has to satisfy the Young–Laplace law, given in equation (A.1). Since equation (A.5) is difficult to solve for (y^i, r^i), the solution is obtained by an iterative procedure for one point after the other. In that way, the shape of the bubble can be computed point-wise. When $y^i - y^{i-1}$ is smaller than 0 for the first time, the upmost point of the surface is found, corresponding to the contact point with the horizontal wall on top, as sketched in figure 4. The corresponding radial position r^{i-1} yields the radius $R_a = r^{i-1}$ of the contact area. The surface of the bubble is assumed to continue with zero curvature, parallel to the horizontal wall and thus, forming a closed

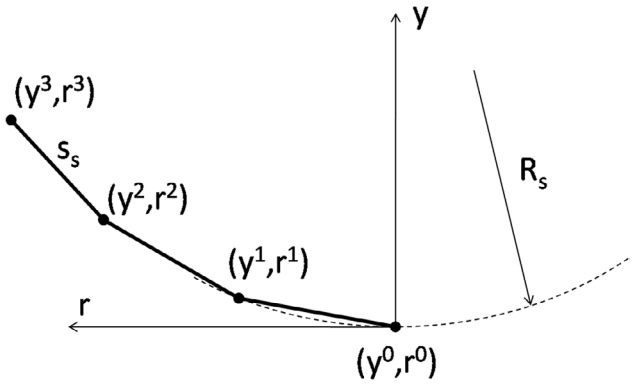

Figure A2. Sketch of the calculation of the bubble shape. The calculation starts at the apex of the bubble with the guessed radius R_s. The distance between two discretisation points is s_s.

surface. According to the Young–Laplace law (A.1) zero curvature corresponds to zero pressure difference. This means, p_{out} at the contact area is not taken from the prescribed outer pressure distribution but is assumed to equal p_{b}. In reality, the pressure difference between p_{out} just outside of the gap and p_{b} inside the gap would either result in a flow from the gap, thinning the lamella or would be counteracted by disjoining pressure [6] between surfactants and the wall, which is not modelled here.

Now, that the surface shape is calculated, the volume of the resulting bubble is computed by

$$V_{\text{b}} = \pi/3 \sum_{i=1}^{\max} (y^i - y^{i-1})(r^{i-1}r^{i-1} + r^i r^{i-1} + r^i r^i). \tag{A.6}$$

The resulting bubble volume is compared to the initially desired one, a new starting value for p_{b} and R_s is derived (figure A1) and the construction of the bubble surface starts over again. In that way, by an outer iteration loop the desired bubble volume is achieved. Summing up, this algorithm allows for computing the equilibrium shape of a bubble of a certain volume V_{b}, exposed to a pressure field p_{out} and placed below a horizontal wall. Subsequently, the centre of mass, the surface area, the contact area and other geometrical measures can be derived from the shape. An example for such a shape is shown in figure 4.

It might be surprising, that this algorithm works so well. It is counter-intuitive, that the point where $y^i - y^{i-1}$ becomes negative actually corresponds to the physically correct contact point with the horizontal wall. In fact, in every loop of the outer iteration a physically correct shape is computed, because each computed shape fulfils the Young–Laplace law. The outer iteration loop only arranges the bubble volume to equal the prescribed one.

After finding a shape, the results can be validated by analysing the equilibrium between the contact force F_{a}, acting on the contact area $r \leqslant R_a$ near the wall, and the fluid force F_{out}, acting along the free surface of the bubble between the apex and the contact point.

$$-F_{\text{out}} = -\int_{\text{free surface}} p_{\text{out}} \mathbf{e}_{\text{n}} dA \cdot \mathbf{e}_y = p_{\text{b}} \pi R_a^2. \tag{A.7}$$

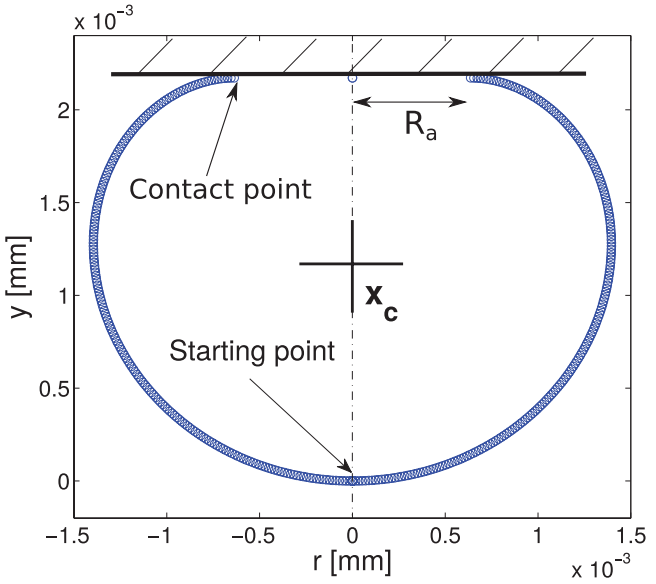

Figure A3. Numerical result of the shape of a bubble colliding with a horizontal wall.

This equilibrium is found to be valid with deviation below 1%. The equilibrium of forces is a very convincing validation of the applied approach. In case of a purely gravitational pressure field $p_{\text{out}} = p_s - \rho_{\text{f}} g y$, also the buoyancy force $F_{\text{b}} = V_{\text{b}} \rho_{\text{f}} g$ can be considered for validation. It has to satisfy

$$F_{\text{b}} = V_{\text{b}} \rho_{\text{f}} g = \int_{\text{free surface}+\text{contact area}} p_{\text{out}} \mathbf{e}_{\text{n}} dA \cdot \mathbf{e}_{\text{y}}, \tag{A.8}$$

which also was found to be valid with a deviation below 0.1%.

After deriving the shape of the bubble, we can derive the y-position of the centre of mass of the bubble $\mathbf{x}_{\text{c}}$. This yields the desired relation between the distance of $\mathbf{x}_{\text{c}}$ from the wall and the acting force $F_{\text{elastic}} = -F_{\text{out}} = F_a$.

Finally, one can compare two shapes of bubbles with the same volume and slightly different fluid forces F_{out}. Applying equation (4), discretizing the derivation with a finite difference, one can carry out yet another validation of the shape computation with $F_{\text{elastic}} = -F_{\text{out}}$.

Appendix B. Estimation of dissipation

In order to derive the energy dissipation in the collision zone, the geometry of the fluid displacement process is further simplified, as sketched in figure B1. The lamella itself is supposed to be a plane disk of radius R_a and height h_0. Next to it appears the dissipation zone, that is bounded by a surface radius of R_{b}. Thus, one can derive the height of the gap in the collision zone as a function of the radial position r, yielding

$$h(r) = h_0 + R_{\text{b}} - \sqrt{R_b^2 - (r - R_a)^2} \tag{B.1}$$

$$\frac{\mathrm{d}h}{\mathrm{d}R_a} = \frac{-(r - R_a)}{\sqrt{R_b^2 - (r - R_a)^2}}. \tag{B.2}$$

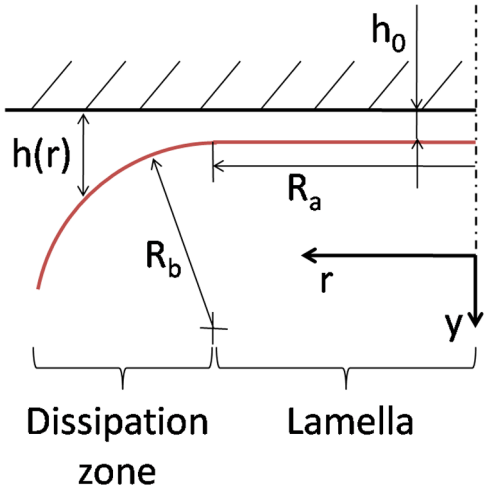

Figure B1. Proposed simplification of lamella geometry during collision. The thickness of the lamella, h_0, remains constant while its radius R_a changes, displacing liquid in the dissipation zone.

When the bubble approaches the wall, R_a increases. The relation between R_a and Δ can be derived from the shape calculations in section 2.2, yielding

$$\frac{R_a}{R_{\mathrm{eq}}} = -30.0 + \sqrt{900.0 + 0.424\frac{\Delta}{R_{\mathrm{eq}}}} \tag{B.3}$$

$$\frac{\mathrm{d}R_a}{\mathrm{d}\Delta} \approx 0.34\sqrt{\frac{\Delta}{R_{\mathrm{eq}}} + 0.0002}\,. \tag{B.4}$$

The radius R_{b} can also be derived from the shape calculator. It equals in good agreement the bubble radius R_{eq}.

The dissipative force F_{viscous}, acting on the bubble in the collision process, can be derived from the energy dissipation rate in the dissipation zone

$$F_{\mathrm{viscous}} = \frac{\mathrm{d}E}{\mathrm{d}\Delta} = \frac{\mathrm{d}E_{\mathrm{dissipate}}}{\mathrm{d}t}\frac{1}{u_{\mathrm{c}}}. \tag{B.5}$$

The energy dissipation results from viscous flow of the displaced fluid in the gap. The volumetric flow through a vertical cross section at a given radial position $r = \tilde{r} \geqslant R_a$ results from the change in gap width h

$$\left.\frac{\mathrm{d}V}{\mathrm{d}t}\right|_{r=\tilde{r}} = u_{\mathrm{c}}\,\frac{\mathrm{d}R_a}{\mathrm{d}\Delta}\left.\frac{\mathrm{d}V}{\mathrm{d}R_a}\right|_{r=\tilde{r}} \tag{B.6}$$

$$\left.\frac{\mathrm{d}V}{\mathrm{d}R_a}\right|_{r=\tilde{r}} = \int_{R_a}^{\tilde{r}} 2\pi r\frac{\mathrm{d}h}{\mathrm{d}R_a}\,\mathrm{d}r \tag{B.7}$$

$$= 2\pi\left(R_a(h-h_0) + \frac{R_{\mathrm{eq}}^2}{2}\mathrm{asin}\left(\frac{(\tilde{r}-R_a)}{R_{\mathrm{eq}}}\right) - \frac{\tilde{r}-R_a}{2}\sqrt{R_b^2 - (\tilde{r}-R_a)^2}\right). \tag{B.8}$$

Assuming, as an approximation, a fully developed, two-dimensional Poiseuille flow in the gap, it is possible to derive the energy dissipation rate

$$\frac{\mathrm{d}E_{\mathrm{dissipate}}}{\mathrm{d}t} = \int_{R_a}^{r_{\max}}\frac{\mathrm{d}p}{\mathrm{d}\tilde{r}}\frac{\mathrm{d}V}{\mathrm{d}t}\,\mathrm{d}\tilde{r} \tag{B.9}$$

$$= \int_{R_a}^{r_{\max}}\frac{\mathrm{d}p}{\mathrm{d}\tilde{r}}\frac{\mathrm{d}V}{\mathrm{d}R_a}\,\mathrm{d}\tilde{r}\,\frac{\mathrm{d}R_a}{\mathrm{d}t}. \tag{B.10}$$

At this point, the assumption of a no-slip bundary condition on the bubble surface and on the obstacle-surface is necessary. The pressure gradient in a Poiseuille flow is

$$\frac{\mathrm{d}p}{\mathrm{d}\tilde{r}} = C_{\mathrm{bc}}\frac{12\eta_{\mathrm{f}}}{2\pi\tilde{r}h^3}\frac{\mathrm{d}V}{\mathrm{d}R_a}\frac{\mathrm{d}R_a}{\mathrm{d}t}. \tag{B.11}$$

The parameter C_{bc} represents the collision partner. For a bubble–wall collision holds $C_{\mathrm{bc}} = 1$, for for a bubble–bubble collision $C_{\mathrm{bc}} = 1/4$. Consequently, the energy dissipation can be written as

$$\frac{\mathrm{d}E_{\mathrm{dissipate}}}{\mathrm{d}t} = C_{\mathrm{bc}}\frac{12\eta_{\mathrm{f}}}{2\pi}\left(\frac{\mathrm{d}R_a}{\mathrm{d}t}\right)^2\int_{R_a}^{R_a+R_{\mathrm{eq}}}\left(\frac{\mathrm{d}V}{\mathrm{d}R_a}\right)^2\frac{1}{\tilde{r}h^3}\,\mathrm{d}\tilde{r}. \tag{B.12}$$

This integral can be solved analytically. However, the result is extremely complex and not at all handy. Therefore, by computing it numerically and fitting the result, the following numerical approximation was found

$$\int_{R_a}^{R_a+R_{\mathrm{eq}}}\left(\frac{\mathrm{d}V}{\mathrm{d}R_a}\right)^2\frac{1}{\tilde{r}h^3}\,\mathrm{d}\tilde{r} \approx 4.0\sqrt{\frac{R_{\mathrm{eq}}^3}{h_0}} + 3.0R_a\frac{R_{\mathrm{eq}}}{h_0}. \tag{B.13}$$

For values $0.1\ \mathrm{mm} < R_{\mathrm{eq}} < 0.3\ \mathrm{mm}$, $1\ \mu\mathrm{m} < h_0 < 100\ \mu\mathrm{m}$, $0 < R_a < R_{\mathrm{eq}}$, equation (B.13) approximates the integral with a deviation smaller than 10 %. This deviation is negligible compared to the modelling uncertainties.

Combining equation (B.5) with the equations (B.12), (B.13), (B.3) and (B.4), one ends up with an expression for the viscous force, acting on a bubble in the collision process

$$F_{\mathrm{viscous}} = u_{\mathrm{c}}C_{\mathrm{bc}}\frac{12\mu_{\mathrm{f}}}{2\pi}0.34\sqrt{\frac{\Delta}{R_{\mathrm{eq}}} + 0.0002}\left(4.0\sqrt{\frac{R_{\mathrm{eq}}^3}{h_0}} + 3.0R_a\frac{R_{\mathrm{eq}}}{h_0}\right). \tag{B.14}$$

This expression only depends on bubble position $\Delta = R_{\mathrm{eq}} - x_{\mathrm{c}}$, bubble velocity u_{c}, bubble radius R_{eq} and fluid viscosity μ_{f}. The lamella thickness h_0 can be estimated with equation (14). The contact radius R_a is given in equation (B.4) and is a function of R_{eq}, and Δ, as well. The force linearly depends on the bubble velocity, which is typical for viscous dissipation mechanisms.

References

[1] Abbena E, Salamon S and Gray A 2006 *Modern Differential Geometry of Curves and Surfaces with Mathematica* (Boca Raton, FL: CRC Press)

[2] Basu A, Xu Y, Still T, Arratia P E, Zhang Z, Nordstrom K N, Rieser J M, Gollub J P, Durian D J and Yodh A G 2014 Rheology of soft colloids across the onset of rigidity: scaling behavior, thermal, and non-thermal responses *Soft Matter* **10** 3027–35

[3] Becker V and Briesen H 2008 Tangential-force model for interactions between bonded colloidal particles *Phys. Rev.* E **78** 061404

[4] Brakke K A 1992 The surface evolver *Exp. Math.* **1** 141–65
[5] Brenner H 1961 The slow motion of a sphere through a viscous fluid towards a plane surface *Chem. Eng. Sci.* **16** 242–51
[6] Cantat I, Cohen-Addad S, Elias F, Graner F, Höhler R and Pitois O 2013 *Foams: Structure and Dynamics* (Oxford: Oxford University Press)
[7] Carvente O, Salazar-Cruz M, Peñuñuri F and Ruiz-Suárez J C 2016 Dynamic self-assembly of non-brownian spheres studied by molecular dynamics simulations *Phys. Rev.* E **93** 020902
[8] Caserta A J, Navarro H A and Cabezas-Gómez L 2016 Damping coefficient and contact duration relations for continuous nonlinear spring-dashpot contact model in dem *Powder Technol.* **302** 462–79
[9] Chan D Y C, Klaseboer E and Manica R 2011 Film drainage and coalescence between deformable drops and bubbles *Soft Matter* **7** 2235–64
[10] Chan D Y C, Klaseboer E and Manica R 2011 Theory of non-equilibrium force measurements involving deformable drops and bubbles *Adv. Colloid Interface Sci.* **165** 70–90
[11] Clift R, Grace J R and Weber M E 1978 *Bubbles, Drops and Particles* (New York: Academic)
[12] Cox R G and Brenner H 1967 The slow motion of a sphere through a viscous fluid towards a plane surface—small gap widths, including inertial effects *Chem. Eng. Sci.* **22** 1753–77
[13] Craster R V and Matar O K 2009 Dynamics and stability of thin liquid films *Rev. Mod. Phys.* **81** 1131
[14] Dagastine R R, Manica R, Carnie S L, Chan D Y C, Stevens G W and Grieser F 2006 Dynamic forces between two deformable oil droplets in water *Science* **313** 210–3
[15] Davis R H, Serayssol J-M and Hinch E J 1986 The elastohydrodynamic collision of two spheres *J. Fluid Mech.* **163** 479–97
[16] Denkov N D, Tcholakova S, Golemanov K, Ananthapadmanabhan K P and Lips A 2008 Viscous friction in foams and concentrated emulsions under steady shear *Phys. Rev. Lett.* **100** 138301
[17] Durian D J 1995 Foam mechanics at the bubble scale *Phys. Rev. Lett.* **75** 4780
[18] Garstecki P, Fuerstman M J, Stone H A and Whitesides G M 2006 Formation of droplets and bubbles in a microfluidic t-junction: scaling and mechanism of break-up *Lab Chip* **6** 437–46
[19] Goldman A J, Cox R G and Brenner H 1967 Slow viscous motion of a sphere parallel to a plane wall 1 motion through a quiescent fluid *Chem. Eng. Sci.* **22** 637–51
[20] Heitkam S, Schwarz S, Santarelli C and Fröhlich J 2013 Influence of an electromagnetic field on the formation of wet metal foam *Eur. Phys. J. Spec. Top.* **220** 207–14
[21] Hendrix M H W, Manica R, Klaseboer E, Chan D Y C and Ohl C-D 2012 Spatiotemporal evolution of thin liquid films during impact of water bubbles on glass on a micrometer to nanometer scale *Phys. Rev. Lett.* **108** 247803
[22] Hilton J E, Mason L R and Cleary P W 2010 Dynamics of gas–solid fluidised beds with non-spherical particle geometry *Chem. Eng. Sci.* **65** 1584–96
[23] Hutzler S, Murtagh R P, Whyte D, Tobin S T and Weaire D 2014 Z-cone model for the energy of an ordered foam *Soft Matter* **10** 7103–8
[24] Hwang H J, Riggleman R A and Crocker J C 2016 Understanding soft glassy materials using an energy landscape approach *Nat. Mater.* **15** 1031–6
[25] Johnson K L 1987 *Contact Mechanics* (Cambridge: Cambridge University Press)
[26] Johnson K L, Kendall K and Roberts A D 1971 Surface energy and the contact of elastic solids *Proc. R. Soc. Lond.* A **324** 301–13
[27] Kempe T and Fröhlich J 2012 Collision modeling for the interface-resolved simulation of spherical particles in viscous fluids *J. Fluid Mech.* **709** 445–89
[28] Kempe T and Fröhlich J 2012 An improved immersed boundary method with direct forcing for the simulation of particle laden flows *J. Comput. Phys.* **231** 3663–84
[29] Kempe T, Vowinckel B and Fröhlich J 2014 On the relevance of collision modeling for interface-resolving simulations of sediment transport in open channel flow *Int. J. Multiph. Flow* **58** 214–35
[30] Ketelaar C and Ajaev V S 2015 Significance of electrically induced shear stress in drainage of thin aqueous films *Phys. Rev.* E **91** 052403
[31] Kruggel-Emden H, Wirtz S and Scherer V 2008 A study on tangential force laws applicable to the discrete element method (dem) for materials with viscoelastic or plastic behavior *Chem. Eng. Sci.* **63** 1523–41
[32] Manica R and Chan D Y C 2011 Drainage of the air–water–quartz film: experiments and theory *Phys. Chem. Chem. Phys.* **13** 1434–9
[33] Manica R, Klaseboer E, Gupta R, Hendrix M H W, Ohl C-D and Chan D Y C 2012 Modelling film drainage of a bubble hitting and bouncing off a surface *9th Int. Conf. on CFD in the Minerals and Process Industries* vol 100 p 024501
[34] Mason T G, Lacasse M-D, Grest G S, Levine D, Bibette J and Weitz D A 1997 Osmotic pressure and viscoelastic shear moduli of concentrated emulsions *Phys. Rev.* E **56** 3150
[35] O'Hern C S, Silbert L E, Liu A J and Nagel S R 2003 Jamming at zero temperature and zero applied stress: the epitome of disorder *Phys. Rev.* E **68** 011306
[36] Podvin B, Khoja S, Moraga F and Attinger D 2008 Model and experimental visualizations of the interaction of a bubble with an inclined wall *Chem. Eng. Sci.* **63** 1914–28
[37] Pushkarova R A and Horn R G 2005 Surface forces measured between an air bubble and a solid surface in water *Colloids Surf.* A **261** 147–52
[38] Pushkarova R A and Horn R G 2008 Bubble–solid interactions in water and electrolyte solutions *Langmuir* **24** 8726–34
[39] Schwarz S, Kempe T and Fröhlich J 2015 A temporal discretization scheme to compute the motion of light particles in viscous flows by an immersed boundary method *J. Comput. Phys.* **281** 591–613
[40] Tcholakova S, Denkov N D, Golemanov K, Ananthapadmanabhan K P and Lips A 2008 Theoretical model of viscous friction inside steadily sheared foams and concentrated emulsions *Phys. Rev.* E **78** 011405
[41] Tsao H-K and Koch D L 1997 Observations of high reynolds number bubbles interacting with a rigid wall *Phys. Fluids* **9** 44–56
[42] Van Hecke M 2009 Jamming of soft particles: geometry, mechanics, scaling and isostaticity *J. Phys.: Condens. Matter* **22** 033101
[43] Vincent F, Le Goff A, Lagubeau G and Quéré D 2007 Bouncing bubbles *J. Adhes.* **83** 897–906
[44] Woldhuis E, Chikkadi V, van Deen M S, Schall P and van Hecke M 2015 Fluctuations in flows near jamming *Soft Matter* **11** 7024–31
[45] Xue J, Chen F, Yang N and Ge W 2016 Eulerian-lagrangian simulation of bubble coalescence in bubbly flow using the spring-dashpot model *Chin. J. Chem. Eng.* (doi:10.1016/j.cjche.2016.08.006)
[46] Yoon Y, Baldessari F, Ceniceros H D and Leal L G 2007 Coalescence of two equal-sized deformable drops in an axisymmetric flow *Phys. Fluids* **19** 102102
[47] Zawala J, Krasowska M, Dabros T and Malysa K 2007 Influence of bubble kinetic energy on its bouncing during collisions with various interfaces *Can. J. Chem. Eng.* **85** 669–78
[48] Zenit R and Legendre D 2009 The coefficient of restitution for air bubbles colliding against solid walls in viscous liquids *Phys. Fluids* **21** 083306